Abdominal Radiology

Published online: 27 August 2018

Abdom Radiol (2019) 44:95–103
https://doi.org/10.1007/s00261-018-1716-8

Skewness of apparent diffusion coefficient (ADC) histogram helps predict the invasive potential of intraductal papillary neoplasms of the bile ducts (IPNBs)

Kai-pu Jin,[1,2,3] Sheng-xiang Rao,[1,2,3] Ruo-fan Sheng,[1,2,3] and Meng-su Zeng[1,2,3]

[1]Department of Radiology, Zhongshan Hospital, Fudan University, No. 180 Fenglin Rd, 200032 Shanghai, China
[2]Shanghai Institute of Medical Imaging, No. 180 Fenglin Rd, 200032 Shanghai, China
[3]Department of Medical Imaging, Shanghai Medical College, Fudan University, Shanghai, China

Abstract

Objective: This retrospective study was to explore the value of whole lesion apparent diffusion coefficient (ADC) histogram in distinguishing invasive and noninvasive intraductal papillary neoplasms of the bile ducts (IPNBs).

Method and materials: Fifty-two patients of IPNB underwent MRI at 1.5T with diffusion-weighted imaging (DWI, $b = 500$ s/mm^2) before surgical resections. ADC histogram metrics were generated by using the software MR OncoTreat. The mean, standard deviation, median, skewness, kurtosis as well as the 10th, 25th, 75th, and 90th percentiles were compared between pathologically defined invasive ($n = 35$) and noninvasive ($n = 17$) IPNBs. Such conventional imaging characters as lesion location, bile duct wall dilation, and mural nodularity were also assessed. Multivariate regression analysis as well as receiver operating characteristics (ROC) analysis were then conducted to determine the predictive factors and to evaluate potential diagnostic performances.

Results: The inter-operator reliability was good to excellent (ICC: 0.693–979). Mean median, kurtosis, and the 10th, 25th, 75th, 90th percentiles were all greater in noninvasive group than invasive ones (P: 0.00–002). Skewness was lower in noninvasive group than invasive ones (-1.0 ± 0.6 vs. -0.3 ± 0.6, $P = 0.00$). After multivariate regression, skewness (AUC = 0.822, 95%CI 0.70–0.91) and mural nodularity (accuracy = 0.808) were the only two independent factors in predicting invasive IPNBs. The diagnostic performance improved (AUC = 0.867, 95%CI 0.742–0.946) when combining skewness and mural nodularity, however, the difference did not reach statistical significance ($P = 0.16$).

Conclusion: The ADC histogram has capability of distinguishing invasive and noninvasive IPNBs, in which skewness was an independent predictive factor.

Key words: Bile duct neoplasms—Cholangiocarcinoma—Neoplasm invasiveness—Diffusion magnetic resonance imaging—Comparative study

Intraductal papillary neoplasm of the bile duct (IPNB) is one of the important precursor lesions of biliary malignancies proposed in recent years [1–3]. On general, it carries a much better prognosis than cholangiocarcinoma whose 5-year survival rate is only 5% after diagnosed [4]. Alarming symptoms like abdominal pain, jaundice, or fever also occasionally occur in early courses among IPNB patients.

IPNB features remarkable dilation of bile ducts, usually with multiple papillary or villous proliferation of neoplasms growing along within. According to 2010 WHO, IPNB displays a wide histological spectrum ranging from low-/mediate-/high-grade dysplasia to invasive carcinoma. Studies indicate that patient prognosis significantly relies on the level of invasiveness [5, 6], and concurrent bile duct resection (BDR) is essential when surrounding bile duct walls are involved, while on the contrary, BDR is not encouraged if the lesion were not associated with invasive carcinoma. [7].

However, an ideal means for evaluating invasiveness of IPNB preoperatively is now still lacking. Laboratory approaches for screening hepatobiliary malignancies like ALK, γ-GT, and CA19-9 lack specificity. Judging inva-

Correspondence to: Meng-su Zeng; *email:* zengmengsu@outlook.com

siveness by simply observing the integrity of bile duct walls on MR imaging has also proven to be suboptimal [8].

Intraductal papillary mucinous neoplasm of pancreas (IPMN) shares many similarities with IPNB, morphologically and histologically [9–11]. Nevertheless, it has not been wildly discussed yet whether criteria on predicting invasiveness of IPMN, including cystic lesion size, mural mass, and dilation of main duct over 1 cm, might be feasible to the assessment of IPNB.

Diffusion-weighted MR imaging (DWI) together with apparent diffusion coefficient (ADC) is currently widely used to characterize malignant lesions throughout the body. It is based on the theory that cellular compactability of solid cancers leads to restriction of the random Brownian motion of water molecules and decreases ADC value [12–14]. There still lie technical difficulties in case of IPNBs, since multiple intramural nodules with different degree of dysplasia can be scattered along the biliary tree. Measurements of a single nodule obtained on only one single slice can hardly reflect the condition of the entire lesion. Additionally, sometimes, IPNB nodules are too small to be precisely traced ROI (region of interest) or detected on DWI.

Histogram analysis is a more sophisticate approach for evaluating tumor heterogeneity [15]. It can pick up different microenvironments that otherwise might be masked by mean values. It allows colliquation within ROI and is able to analyze the difference [16, 17]. Studies showed ADC histogram analysis might serve as a biomarker for identifying the malignant potential [18–20].

Our study tries exploring IPNB characteristics using ADC histogram and assess its invasive potential.

Materials and methods

This retrospective study was approved by the Institutional Review Board.

Patients selection

By reviewing the database of the Department of Pathology, all patients (n = 101) pathologically diagnosed "IPNB" or "cholangiocarcinoma considered transformed from IPNB" between January 2008 to June 2017 were collected. Patients with no MR examinations before surgeries (n = 23), those who just underwent cholangioscopy but no surgery resection (n = 7), patients who had previous hepatobiliary surgeries (n = 4) were excluded. Among the remaining 67 patients, fifteen cases were excluded because of the poor conspicuity of diffusion-weighted imaging. Finally, 52 patients of IPNB were included. They all underwent routine MRI examinations, including T1WI, T2WI, MRCP, DWI, as well as dynamic contrast-enhanced MR Imaging, within 1 month before surgery. Complete hospital records, radiologic images, surgical records, and pathological reports were also available among all patients(Fig. 1).

MRI technique

All images were obtained on a 1.5T MRI scanner (Avanto; Siemens, Erlangen, Germany) in the transverse plane with a posterior spine array coil and an anterior body phased array coil. The conventional abdominal MR protocol consisted as follows: (1) axial respiratory-navigated T2-weighted fat-suppressed turbo-spin-echo (TSE) sequence [repetition time (TR)/echo time (TE) = 3500/84 ms; slice thickness = 5 mm; slice gap = 1 mm; field of view (FOV) optimized to patients' body habitus: 285 × 214–308 × 380 mm; matrix = 168 × 320]; (2) in- and opposed-phase axial T1WI sequence [TR/TE = 6.8/2.35 (in-phase), 4.75 (opposed-phase) msec; slice thickness = 5 mm; slice gap = 1 mm; FOV = 85 × 214–308 × 380 mm; matrix = 180 × 320]; (3) DWI (b = 0, 500 s/mm^2) sequence with a free-breathing single-shot echo-planar technique [TR/TE = 3400/70 ms, slice thickness = 6 mm, slice gap = 1.8 mm, matrix = 128 × 80]. Corresponding ADC maps were automatically generated. (4) The coronal and coronal oblique thick-slab single-section T2-weighted MRCP using fast or turbo SE technique breath-holding [TR/TE = 4500/758 ms; slice thickness = 40 mm; FOV = 340 × 340 mm; matrix = 180 × 320]; (5) Coronal thin-slab multi-section T2-weighted MRCP using single-shot fast SE sequence or the half-Fourier rapid acquisition with relaxation enhancement sequence during breath-holding [TR/TE = 1240/88 ms, slice thick-

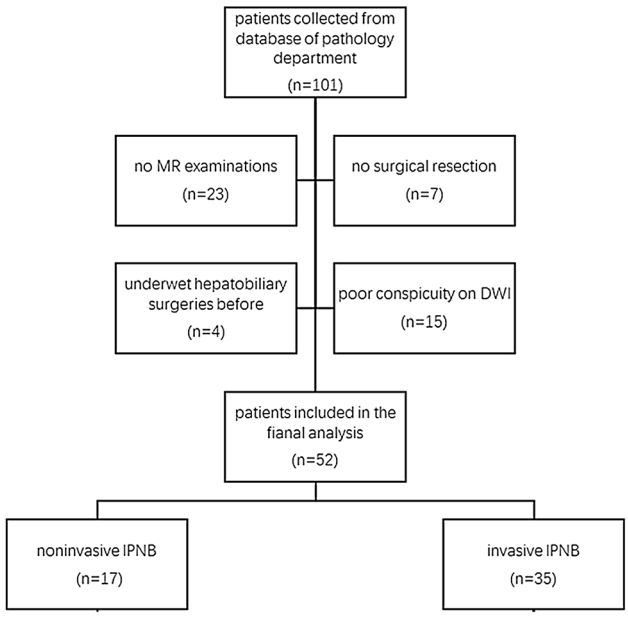

Fig. 1. Flow chart showing patient selection criteria.

ness = 4 mm, slice gap = 20 mm, FOV = 280 × 320 mm; matrix = 180 × 320].

Image analysis

All the MR images were reviewed on PACS (Pathspeed, GE Medical Systems Integrated Imaging Solutions, Prospect, IL). Two radiologists (Z.M.S with 33 years and J.K.P with 5 years abdominal imaging experience) were trained to decipher the MR morphological features of IPNB blinded to pathology and clinical data, including the location of lesion, the mural nodularity, and measure the lesion size. The evaluation of mural nodularity was mainly performed on T2WI and MRCP where filling defects were observed and further confirmed on T1WI or dynamic contrast enhancement (DCE) series in differentiation with biliary lithiasis. Different results were allowed to be further discussed between the two reviewers to reach an agreement. Sizes were measured on transversal T2WI by recording the maximum diameter of the dilated bile ducts.

Histogram analyses

A prototype software (MR OncoTreat, Siemens Healthcare) was used in histogram analysis. On ROI (region of interest) definition, we segmented the entire lesion along its borders on axial images as well as on software-generated coronal and sagittal images of DWI, in reference with the original sagittal slices of T2WI. In general rule, gallbladder and biliary stones are not included; peripheral hepatic parenchyma is not included within ROIs; but the main body of the lesion need be included to the surrounding bile duct walls; visible but very tiny branches near targeted apparently dilated branches the can be omitted if precision is difficult to acquire. Manual selection adding semi-automated adaptive thresholding techniques was then used in our ROI definition [21]. The software automatically copied the ROIs to the corresponding ADC maps (Figs. 2, 3) and generated a histogram on which the whole lesion's mean, standard deviation, median, skewness, and kurtosis were acquired directly and the 10th, 25th, 75th, 90th percentile value of ADCs were recorded by sliding the value bars. The ROI mapping and histogram measurements were conducted by two radiologists (Z.M.S with 33 years and J.K.P with 5 years abdominal imaging experience) independently blinded to pathological findings.

Statistical analyses

All analyses were performed with the software of SPSS 22 for Windows X64; SPSS Inc., Chicago, IL in our study. Reliability of ADC histogram measurement was defined using interclass correlation coefficient (ICC. poor, < 0.4; fair, 0.4–0.59; good, 0.6–0.74; excellent, 0.75–1.0) [22]. Clinical information, conventional imaging assessment, and ADC histogram parameters were all compared between invasive and noninvasive IPNB groups. Continuous variables were compared using Student's t test if K–S test proved its normality and otherwise using Mann–Whitney U-test. Categorical variables were compared using Pearson's Chi-squared test of Fisher's exact test. Any variables with $P < 0.0.5$ after the analyses were then substituted to multivariate logistic regression analysis, using a forward entering method, in constructing the final model with a significance level of > 0.05 for removal. The left variables in the model were considered independent predictors for invasive IPNBs. Diagnostic performance was assessed by receiver operating characteristics (ROC) analysis. The area under curve (AUC) was calculated and compared using DeLong et al. test. Appropriated cutoff values were also obtained with sensitivity, specificity, positive predictive value, and negative predictive value for invasiveness evaluation calculated as well. All tests in our study were two-sided. A difference of P value under 0.05 was considered statistically significant.

Results

Patient characteristics and conventional imaging assessment

A total of 52 patients, 28 male (53.8%) and 24 female (41.2%) aged 62 ± 8 years, meeting all the criteria were included. Clinical information of our patients was detailed as Table 1.

Among all 52 IPNBs, 17 cases were pathologically defined as noninvasive IPNBs, including 7 cases of low to intermediate dysplasia and 10 cases of high-grade dysplasia. 35 others were defined as invasive IPNB, including 6 cases with micro foci invasion and 29 cases with macro invasion. CA19-9 was higher in invasive group (51.7, 95%CI 10.4–208.4) than the noninvasive group (18.4, 95%CI 7.9–27.9). Total bilirubin was higher in noninvasive group (13.5, 95%CI 9.5–32.5) than the invasive one (10, 95%CI 7.5–13.0). No significant differences were found on age, gender, onset symptoms, and preoperative laboratory results between the two groups.

In conventional imaging assessment, invasive IPNBs were more likely to show intramural nodules than noninvasive group (33/38 vs. 8/17, accuracy = 0.808, $P < 0.001$). However, neither location nor the extent of bile ducts dilation was related to invasiveness ($P > 0.05$).

Histogram analysis

The results of histogram analysis indicated that the mean, median ADCs, kurtosis of the histogram as well as the 10th, 25th, 75th, 90th percentile values were all significantly lower in invasive IPNBs than in noninvasive IPNBs ($P < 0.05$). Skewness of the invasive group had a significantly less negative value than the noninvasive

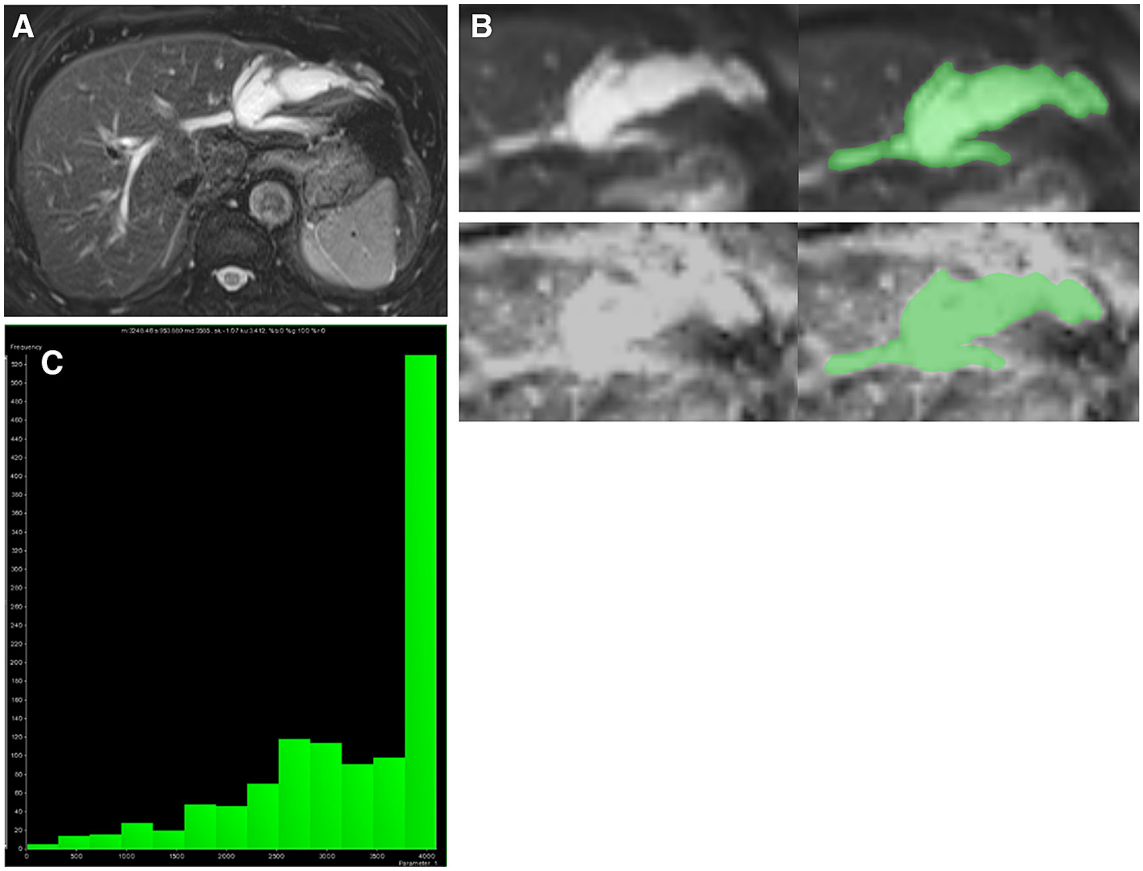

Fig. 2. A 66-year-old male with noninvasive IPNB (intermediate grade of dysplasia pathologically). **A** Axial T2WI revealed diffused dilation of the biliary tree, especially in the left lobe. No intramural nodules were found within the lesion. **B** One of the slices of DWI and the corresponding ADC map. ROI was traced along the border of lesion on DWI, and was copied to the same area of ADC map. Both DWI and ADC maps showed hyper intensity at lesion areas. **C** Histogram of ADC values with a left-side distribution (descriptive analysis reports: mean: $3.248 \times 10^{-3}mm^2/s$, standard deviation: 0.953×10^{-3}, median: $3.585 \times 10^{-3}mm^2/s$, skewness: -1.07, kurtosis: 3.412) and an extremely high peak near the maximum value representing mucin producing.

group (-0.3 ± 0.6 vs. -1.0 ± 0.6, $P < 0.001$). Standard Deviation was the only parameter without showing significant difference between the two groups ($P = 0.328$). Detailed statistical analysis is shown in Table 2.

We included all significant variables, into multivariate logistic regression analysis. Results showed that skewness and the presence of intramural nodules were both independent predictive factors for IPNB invasiveness, with odds ratio of 4.527 and 7.232, respectively (Table 3).

ROC curves were used to compare the significant items in the multivariate regression. The corresponding AUCs, sensitivities, specificities, PPVs NPVs, and cutoff values are shown in Table 3. At the cutoff value of > -0.739, the sensitivity and specificity in predicting invasiveness was 80% (95%CI 63.1–91.6%) and 70.59% (95%CI 32.9–81.6%), respectively. Mural nodularity reached an optimal sensitivity of 94.29% (95%CI 80.8–99.3%), however, its specificity was a fair 52.94% (95%CI 27.8–77.0%). The AUC of the combined ROC of skewness and mural nodularity (AUC = 0.867, 95%CI 0.742–0.946) was greater than sheer AUC of skewness (AUC = 0.822, 95%CI 0.70–0.91). However, the difference did not reach statistical significance ($P = 0.16$) (Fig. 4). We also calculated the combined AUC of mural nodularity and CA19-9 level (AUC = 0.820, 95%CI 0.687–0.914). No statistical difference was found between the combined AUC with mural nodularity alone ($P = 0.28$) or skewness ($P = 1.0$).

The inter-operator reliability of ADC histogram measurements appeared to be good or excellent, with interclass correlation coefficients: mean 0.947, SD 0.809, median 0.953, skewness 0.778, kurtosis 0.693, 10th percentiles 0.902, 25th percentile 0.945, 75th percentile 0.979, 90th percentile 0.946.

Table 1. Comparison between invasive and noninvasive IPNBs in clinical data, conventional imaging assessment, and ADC histogram analysis

	All patients	Invasiveness		*P* value
		−	+	
Number	52	17	35	
Clinical information				
Age (year), median (range)	62 (27–77)	65 (46–77)	61 (27–77)	0.368
Gender, male/female (*n*)	28/24	11/6	17/18	0.376
Symptoms (absent/present)	22/30	4/13	18/17	0.076
CA19-9 (U/mL), median (25%, 75%)	24.9 (9.1, 96.6)	18.4 (7.9,27.9)	51.7 (10.4,208.4)	0.011
TB (umol/L)	11.4 (8.3,25.0)	13.5 (9.6,32.5)	10 (7.5,13.0)	0.033
ALT (U/L)	21 (17,57)	18 (17,60)	20 (17,55)	0.604
AST (U/L)	22 (20,38)	20 (18,40)	22 (20,37)	0.867
γ-GT (U/L)	130 (71,217)	143 (62,382)	137 (73,206)	0.559
ALK (U/L)	119 (85,208)	139 (82,208)	119 (91,259)	0.840
Conventional imaging assessment				
Mural nodules (invisible/visible)	11/41	9/8	2/33	< 0.001
Location: right/left/hilar/distal common bile duct/diffused	8/25/13/1/5	1/9/4/0/3	7/16/9/1/2	0.057
Maximum diameter of dilated bile ducts on transversal section	2.43 (1.73,3.28)	2.30 (1.77,2.50)	2.51 (1.54,3.77)	0.316
Histogram analysis				
Mean ($\times 10^{-3}$mm^2/s)	/	(3.1 ± 0.3)	(2.6 ± 0.6)	0.000
Standard deviation	/	(0.90 ± 0.12)	(0.87 ± 0.16)	0.328
Median ($\times 10^{-3}$mm^2/s)	/	(3.4 ± 0.5)	(2.6 ± 0.7)	0.000
Skewness	/	− 1.0 ± 0.6	− 0.3 ± 0.6	0.000
Kurtosis	/	3.41 (2.26,4.78)	2.78 (2.51,3.37)	0.013
10th percentile ($\times 10^{-3}$mm^2/s)	/	(1.9 ± 0.4)	(1.4 0.6)	0.002
25th percentile ($\times 10^{-3}$mm^2/s)	/	(2.6 ± 0.5)	(2.0 ± 0.6)	0.001
75th percentile ($\times 10^{-3}$mm^2/s)	/	4.10 (3.70,4.10)	3.36 (2.76,4.04)	0.001
90th percentile ($\times 10^{-3}$mm^2/s)	/	4.10 (4.08,4.10)	4.06 (3.38,4.10)	0.020

Lab tests results were all obtained at present before any procedures like PTCD, cholangioscopy, or surgery. Data with normal distribution were expressed with 'mean ± standard deviation (SD)'; data with nonnormal distribution were expressed with 'median (the 25th percentile, the 75th percentile)

Table 2. Univariate analysis and multiple regressions between invasive and noninvasive IPNBs

Variables	Univariate analysis	Multiple regression analysis		
	P value	Odds ratio	95%CI	*P* value
CA19-9 (U/mL)	0.011			0.576
TB (umol/L)	0.033			0.072
Mural nodularity	< 0.001	9.296	1.537–5.778	0.041
Mean	< 0.001			0.701
SD	0.328			–
Median	< 0.001			0.635
Skewness	< 0.001	4.366	1.305–15.230	0.020
Kurtosis	0.013			0.924
10th percentile	0.002			0.254
25th percentile	0.001			0.586
75th percentile	0.001			0.900
90th percentile	0.020			0.692

95%CI 95% confidential interval

Discussion

This was the first time the invasiveness of IPNB was discussed in quantitative analysis preoperatively. Our preliminary findings suggested the ADC histogram analysis had good capability for prediction of IPNB invasiveness.

Skewness, a measure of asymmetry of the probability distribution of histogram pattern [15], was an independent predictive factor in our study, with the best diagnostic performance in identifying invasive IPNB (AUC = 0.822, 95%CI 0.70–0.91). Quite a few studies have discussed the efficacy of skewness in malignancy assessment, revealing that higher skewness might suggest better outcomes [21, 23, 24]. In our study, higher skewness was also related to benign lesions. However, in most studies discussing solid tumors, skewness values were positive, while in our study, the average value in both

Table 3. Diagnostic performance in assessing invasiveness of IPNBs by receiver operating characteristics (ROC) analyses

	AUC or accuracy	95%CI	Sensitivity (%)	95%CI	Specificity (%)	95%CI	+ LR	−LR	Cutoff
Skewness			100	90.0–100.0	0	0.0–19.5	1	/	≥ − 2.088
			100	90.0–100.0	17.65	3.8–43.4	1.21	0	> − 1.966
			94.29	80.8–99.3	17.65	3.8–43.4	1.14	0.32	> − 1.649
			94.29	80.8–99.3	35.29	14.2–61.7	1.46	0.16	> − 1.243
			91.43	76.9–98.2	35.29	14.2–61.7	1.41	0.24	> − 1.142
			91.43	76.9–98.2	58.82	32.9–81.6	2.22	0.15	> − 0.943
			80	63.1–91.6	58.82	32.9–81.6	1.94	0.34	> − 0.76
	0.822	0.70–0.91	80	63.1–91.6	70.59	32.9-81.6	2.72	0.28	> − 0.739
			71.43	53.7–85.4	70.59	44.0–89.7	2.43	0.4	> − 0.634
			71.43	53.7–85.4	76.47	50.1–93.2	3.04	0.37	> − 0.623
			65.71	47.8–80.9	76.47	50.1–93.2	2.79	0.45	> − 0.399
			65.71	47.8–80.9	82.35	56.6–96.2	3.72	0.42	> − 0.374
			60	42.1–76.1	82.35	56.6–96.2	3.4	0.49	> − 0.332
			60	42.1–76.1	88.24	63.6–98.5	5.1	0.45	> − 0.303
			45.71	28.8–63.4	88.24	63.6–98.5	3.89	0.62	> − 0.172
			45.71	28.8–63.4	100	80.5–100.0	/	0.54	> − 0.099
			0	0.0–10.0	100	80.5–100.0	/	1	> 0.679
Mural nodularity	0.808	/	94.29	80.8–99.3	52.94	27.8–77.0	2	0.11	/
Combined	0.867	0.742–0.946	88.24	72.5–96.7	76.47	50.1–93.2	4.08	0.16	> 0.661

AUC area under the ROC curve, *+LR* positive likelihood ratio, *−LR* negative likelihood ratio, *95%CI* 95% confidential interval

invasive (-0.3 ± 0.6) and noninvasive (-1.0 ± 0.6) groups were negative, demonstrating an elongated left-tailed distribution of histogram (Figs. 2, 3). This may due to the compound of bile fluids and mucin secreted by IPNBs, which permitted freer Brown motion of water molecules accounting for higher ADC values. Therefore, we supposed the significantly less negative skewness of invasive IPNB might infer the heterogeneous mix of more compact cellular architecture of malignant components into the compound, which decreased the overall ADC value and shifted the histogram pattern to the left. In addition, recent pathological findings indicated that IPNB with more aggressive feature or atypical histology was related to less tendency of hypersecretion, which reduced the amount of mucin within lesion, making the distribution even less negatively skewed [25].

There were controversies on ADC's potential in predicting invasiveness [8, 26]. Two previous studies merely measured the mean ADC values of visible nodules, thus neglecting lesions with no visible mural nodules. In this study, however, we measured the 3D-whole lesion ADC histogram, including every slice of all IPNB lesions regardless of the visibility of solid components, which was supposed to provide more sophisticated and stable results. We found that invasive IPNBs had lower mean, median, and ADC percentiles than noninvasive ones. This might reflect that invasive IPNBs were of more pixels in the lower ADC range, possibly due to more cellularity. In addition, smaller percentiles were usually more associated with solid components within lesions. The 10th ($(1.9 \pm 0.4)mm^2/s$ vs. $(1.4 \pm 0.6)mm^2/s$, $P = 0.002$) or 25th ($(2.6 \pm 0.5)mm^2/s$ vs. $(2.0 \pm 0.6)mm^2/s$, $P = 0.001$) percentiles for invasive IPNBs were lower than noninvasive group. This is consistent to our knowledge that benign or borderline IPNBs lesions grew villous or fronds-like neoplasms, indicating a loose histological nature, while typical papillary cholangiocarcinomas had a more condense or tight cellular structure [27–29].

Invasive IPNB was also associated with a relatively lower kurtosis (2.777 vs. 3.405, $P = 0.013$). A relatively flatter distribution of ADC histogram may infer complexity and heterogeneity of the invasive group. However, it seemed kurtosis (ICC = 0.693) not to be as stable as skewness, percentiles, and other parameters. So it might need further investigation for ascertaining its effeteness, or ways of measurement needed further improvements.

IPNB was usually compared with IPMN. In our study, the mural nodularity was also an important predictive factor for invasiveness, which was consistent with the criteria for malignant IPMN and other cyst-forming tumors [18, 30–34]. Mural nodularity reached a very good sensitivity of 94.29% and was easier to depict, but less time consuming than ADC histogram analysis. In clinical practice, when we come across IPNBs with intramural nodules, invasiveness should be highly suspected. As for cases with no intramural nodules, further ADC histogram analysis might help.

There was a mild to dramatic increase of CA19-9 in invasive IPNBs (62 (12.1,208.4) U/mL) but CA19-9 was normal in noninvasive groups (17.5 (8.5,25.4) U/mL). However, the diagnostic model in combination of CA19-9 and mural nodularity did not achieved a significantly better performance than mural nodularity alone ($P = 0.28$).

The diameters of affected bile ducts were not associated with invasive IPNBs, though in IPMN the dilation of main pancreatic duct was an important sign of carcinoma. In our study, the total bilirubin of noninvasive group (13.45 (9.6,32.5) umol/L) was also higher than the invasive group (10 (7.5,13) umol/L). Yet, the values were both within the normal range, lacking clinical significance. The location of the lesions and the

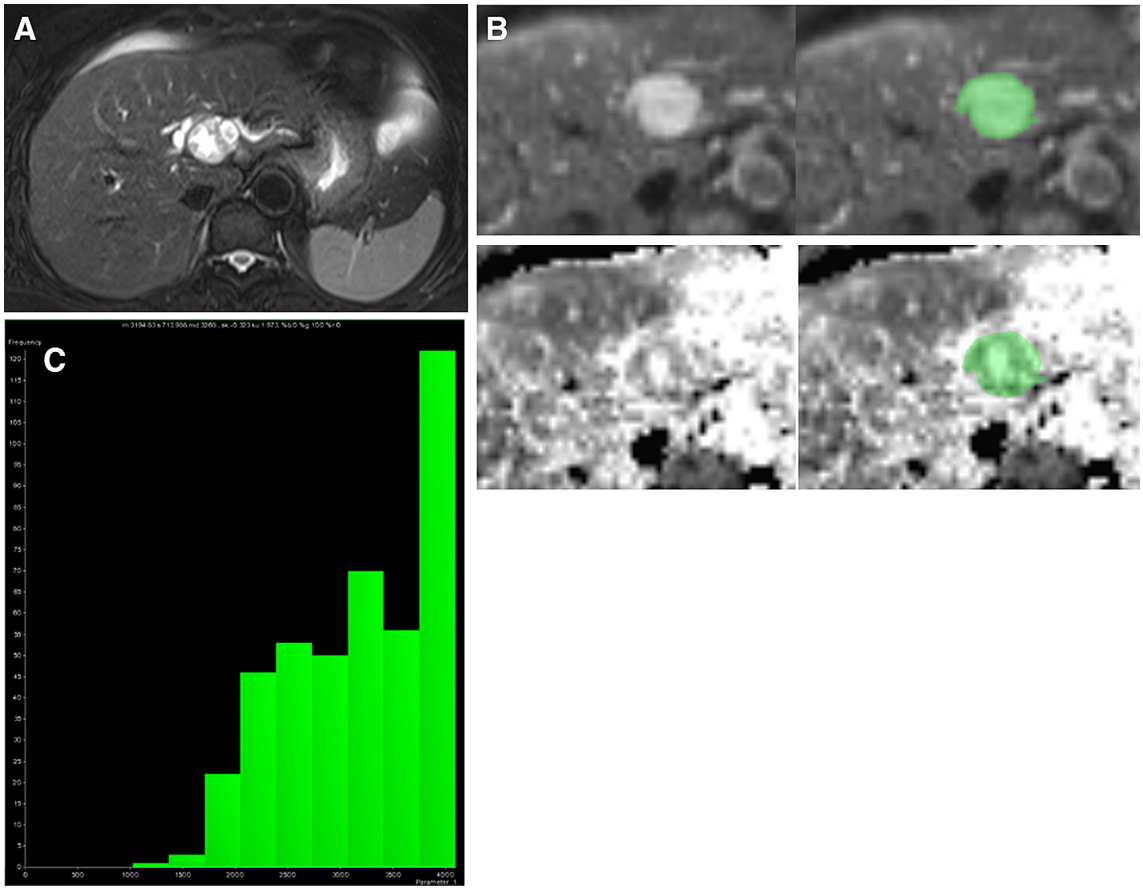

Fig. 3. A 60-year-old female with invasive IPNB (foci associated with adenocarcinoma, all layers of bile ducts infiltrated). **A** Axial T2WI demonstrated local dilation of affected bile ducts. Mural nodules were visible within the lesion. **B** One of the slices of DWI and the corresponding ADC map. ROI was traced along the border of lesion on DWI, and was copied to the same area of ADC map. DWI showed hyper intensity at lesion area, while ADC signal was heterogeneous. **C** Histogram of ADC values with a left-side distribution (descriptive analysis reports: mean: $3.195 \times 10^{-3}mm^2/s$, standard deviation: $0.714 \times 10^{-3}mm^2/s$, median: $3.268 \times 10^{-3}mm^2/s$, skewness: -0.323, kurtosis: 1.973). A high peak was also seen near the maximum value indicating the property of mucin-secreting.

dilation of affected bile ducts were also statistically insignificant.

Binary logistic regression analysis demonstrated that the mural nodularity and skewness being over -0.739 were both independent predictive factors of invasive IPNBs. The conventional image assessment (OR = 9.296) had higher odds ratio than histogram analysis (OR = 4.366), and would achieve a significantly increased AUC (AUC-nodule = 0.736 vs. AUC-combined = 0.867, $P = 0.0108$) when combined with skewness (AUC-skewness = 0.822). Yet there was no significant difference between AUC-skewness and AUC-combined. Considering convenience and efficacy, the conventional assessment was still a competitive means for screening invasive IPNB. However, qualitative assessment relied much on radiologists' experience and image quality. The quantitative ADC histogram analysis might provide a more standardized reference for the diagnosis. Additionally, since histogram analysis reflected the internal organization of the lesion, would it be interesting to further investigate in relation to rumor grade and histological subtypes. It was the first time for histogram analysis applied to the biliary disease and we found the approach feasible and satisfactory for evaluation.

Our study has several limitations. Firstly, the samples size was small. Fifteen cases were excluded because of poor conspicuity. Only 17 out of 52 cases (32.7%) were noninvasive IPNVs, though the rate of morbidity was about the same among general population [25]. Secondly, it was difficult and complicated to precisely draw ROIs when encountered lesions with diffusedly dilated bile ducts because such ROIs were irregular. Standard deviation, skewness, and kurtosis might be operator-dependent to some extent; they had relatively lower ICCs than other parameters. Thirdly, b value was 500 s/mm^2 in our article; no other b values were tested and compared.

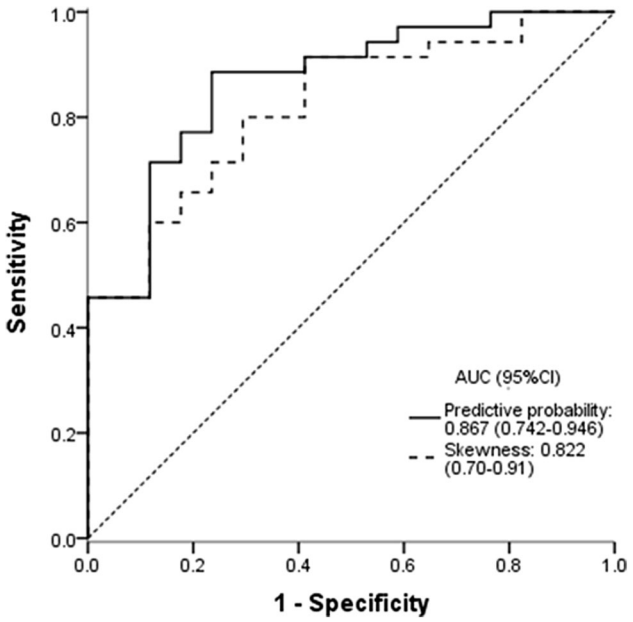

Fig. 4. Receiver operating characteristic (ROC) and area under the curve (AUC) with 95% CI of the skewness of ADC compared with ROC and AUC of the combined skewness and mural nodularity for identification of invasive IPNBs.

In summary, the ADC histogram had potential for distinguishing invasive and noninvasive IPNBs. Especially skewness was an independent predictive factor for the assessment.

Compliance with ethical standards

Conflict of interest The authors of this manuscript declare no relationships with any companies, whose products or services may be related to the subject matter of the article.

Funding The authors state that this work has not received any funding.

Ethical approval All procedures performed in studies involving human participants were in accordance with the ethical standards of the institutional Review Board and with the 1964 Helsinki declaration and its later amendments or comparable ethical standards. This article does not contain any studies with animals performed by any of the authors.

Informed consent Written informed consent was waived by the Institutional.

References

1. Nakanuma Y, Miyata T, Uchida T (2016) Latest advances in the pathological understanding of cholangiocarcinomas. Expert Rev Gastroenterol Hepatol 10(1):113–127
2. Nakanuma Y, Kakuda Y (2015) Pathologic classification of cholangiocarcinoma: new concepts. Best Pract Res Clin Gastroenterol 29(2):277–293
3. Nakanuma Y, Tsutsui A, Ren XS, et al. (2014) What are the precursor and early lesions of peripheral intrahepatic cholangiocarcinoma? Int J Hepatol 2014:805973
4. Mondal D, Silva MA, Soonawalla Z, Wang LM, Bungay HK (2016) Intraductal papillary neoplasm of the bile duct (IPN-B): also a disease of western Caucasian patients. A literature review and case series. Clin Radiol 71(1):e79–e87
5. Luvira V, Pugkhem A, Bhudhisawasdi V, et al. (2016) Long-term outcome of surgical resection for intraductal papillary neoplasm of the bile duct. J Gastroenterol Hepatol. 32(2):527–533
6. Nakanuma Y, Miyata T, Uchida T, Uesaka K (2016) Intraductal papillary neoplasm of bile duct is associated with a unique intraepithelial spreading neoplasm. Int J Clin Exp Pathol 9:11129–11138
7. Perez Saborido B, Bailon Cuadrado M, Rodriguez Lopez M, et al. (2017) Intraductal papillary neoplasia of the bile duct with malignancy: a differentiated entity of cholangiocarcinoma with a better prognosis. A review of three new cases. Revista espanola de enfermedades digestivas 109(8):592–595
8. Yoon HJ, Kim YK, Jang KT, et al. (2013) Intraductal papillary neoplasm of the bile ducts: description of MRI and added value of diffusion-weighted MRI. Abdom Imaging 38(5):1082–1090
9. Zen Y, Fujii T, Itatsu K, et al. (2006) Biliary papillary tumors share pathological features with intraductal papillary mucinous neoplasm of the pancreas. Hepatology 44(5):1333–1343
10. Rocha FG, Lee H, Katabi N, et al. (2012) Intraductal papillary neoplasm of the bile duct: a biliary equivalent to intraductal papillary mucinous neoplasm of the pancreas? Hepatology 56(4):1352–1360
11. Nakanuma Y, Kakuda Y, Uesaka K, et al. (2016) Characterization of intraductal papillary neoplasm of bile duct with respect to histopathologic similarities to pancreatic intraductal papillary mucinous neoplasm. Hum Pathol 51:103–113
12. Jang KM, Kim SH, Min JH, et al. (2014) Value of diffusion-weighted MRI for differentiating malignant from benign intraductal papillary mucinous neoplasms of the pancreas. AJR Am J Roentgenol 203(5):992–1000
13. Kang KM, Lee JM, Shin CI, et al. (2013) Added value of diffusion-weighted imaging to MR cholangiopancreatography with unenhanced mr imaging for predicting malignancy or invasiveness of intraductal papillary mucinous neoplasm of the pancreas. J Magn Reson Imaging 38(3):555–563
14. Curvo-Semedo L, Lambregts DM, Maas M, et al. (2012) Diffusion-weighted MRI in rectal cancer: apparent diffusion coefficient as a potential noninvasive marker of tumor aggressiveness. J Magn Reson Imaging 35(6):1365–1371
15. Just N (2014) Improving tumour heterogeneity MRI assessment with histograms. Br J Cancer 111(12):2205–2213
16. Shukla-Dave A, Lee NY, Jansen JF, et al. (2012) Dynamic contrast-enhanced magnetic resonance imaging as a predictor of outcome in head-and-neck squamous cell carcinoma patients with nodal metastases. Int J Radiat Oncol Biol Phys 82(5):1837–1844
17. Tozer DJ, Jäger HR, Danchaivijitr N, et al. (2007) Apparent diffusion coefficient histograms may predict low-grade glioma subtype. NMR Biomed 20(1):49–57
18. Hoffman DH, Ream JM, Hajdu CH, et al. (2017) Utility of whole-lesion ADC histogram metrics for assessing the malignant potential of pancreatic intraductal papillary mucinous neoplasms (IPMNs). Abdominal radiology. 42(4):1222–1228
19. Rosenkrantz AB (2013) Histogram-based apparent diffusion coefficient analysis: an emerging tool for cervical cancer characterization? AJR Am J Roentgenol 200(2):311–313
20. Downey K, Riches SF, Morgan VA (2013) Relationship between imaging biomarkers of stage I cervical cancer and poor-prognosis histologic features: quantitative histogram analysis of diffusion-weighted MR images. AJR Am J Roentgenol 200:314–320
21. Zolal A, Juratli TA, Linn J, et al. (2016) Enhancing tumor apparent diffusion coefficient histogram skewness stratifies the postoperative survival in recurrent glioblastoma multiforme patients undergoing salvage surgery. J Neuro-oncol 127(3):551–557
22. Cicchetti Domenic V (1994) Guidelines, criteria, and rules of thumb for evaluating normed and standardized assessment instruments in psychology. Psychol Assess 6(4):284–290
23. Kyriazi S, Collins DJ, Messiou C, et al. (2011) Metastatic ovarian and primary peritoneal cancer: assessing chemotherapy response with diffusion-weighted MR imaging—value of histogram analysis of apparent diffusion coefficients. Radiology 261(1):182–192
24. Kamiya A, Murayama S, Kamiya H, et al. (2014) Kurtosis and skewness assessments of solid lung nodule density histograms: differentiating malignant from benign nodules on CT. Jpn J Radiol 32(1):14–21

25. Fukumura Y, Nakanuma Y, Kakuda Y, et al. (2017) Clinicopathological features of intraductal papillary neoplasms of the bile duct: a comparison with intraductal papillary mucinous neoplasm of the pancreas with reference to subtypes. Virchows Archiv 471(1):65–76
26. Jin KP, Sheng RF, Rao SH, et al. (2017) Value of MRI in assessing the invasiveness of intraductal papillary neoplasms of the bile duct. Chin J Radiol 51(8):592–596
27. Liu Y, Zhong X, Yan L, et al. (2015) Diagnostic performance of CT and MRI in distinguishing intraductal papillary neoplasm of the bile duct from cholangiocarcinoma with intraductal papillary growth. Eur Radiol 25(7):1967–1974
28. Ogawa H, Itoh S, Nagasaka T, et al. (2012) CT findings of intraductal papillary neoplasm of the bile duct: assessment with multiphase contrast-enhanced examination using multi-detector CT. Clin Radiol 67(3):224–231
29. Kim JE, Lee JM, Kim SH, et al. (2010) Differentiation of intraductal growing-type cholangiocarcinomas from nodular-type cholangiocarcinomas at biliary MR imaging with MR cholangiography. Radiology 257(2):364–372
30. Kim SH, Lee JM, Lee ES, et al. (2015) Intraductal papillary mucinous neoplasms of the pancreas: evaluation of malignant potential and surgical resectability by using MR imaging with MR cholangiography. Radiology 274(3):723–733
31. Kang HJ, Lee JM, Joo I, Hur BY, et al. (2016) Assessment of malignant potential in intraductal papillary mucinous neoplasms of the pancreas: comparison between multidetector CT and MR imaging with MR cholangiopancreatography. Radiology 279(1):128–139
32. Soares KC, Arnaoutakis DJ, Kamel I, et al. (2014) Cystic neoplasms of the liver: biliary cystadenoma and cystadenocarcinoma. J Am Coll Surg 218(1):119–128
33. Wood CG 3rd, Stromberg LJ 3rd, Harmath CB, et al. (2015) CT and MR imaging for evaluation of cystic renal lesions and diseases. Radiographics 35(1):125–141
34. Park SB, Lee JB (2014) MRI features of ovarian cystic lesions. J Magn Reson Imaging 40(3):503–515